(Preprint) AAS XX-XXX

IMUFDIR Tuning In Response To Structural Deformation Of The Orion Capsule

Nicholas Rahaim[†] and Brandon Wood[‡]

During system level Thermal Vacuum (TVAC) testing it was discovered that the pressure differential of the crew cabin in a vacuum would deflect the capsule slightly, causing significant misalignment of Orion's three Inertial Measurement Units (IMUs). This phenomenon has been likened to a balloon expanding. When this misalignment was modeled in simulation as a function of atmospheric pressure, it was determined that the rate of deflection on reentry was significant enough to cause a mis-compare of the angular rates measured by the IMUs. This mis-comparison of the rates caused Orion's Fault Detection Isolation and Recovery (FDIR) algorithm to falsely fail one of the IMUs. This manuscript will discuss how the IMUFDIR algorithm was detuned to be insensitive to these ballooning effects, while still meeting FDIR requirements to capture real faults in an IMU. All testing to validate this detuning was performed in a Six Degree of Freedom (6 DOF) Monte Carlo Simulation Environment.

INTRODUCTION

In Thermal and Vacuum (TVAC) testing performed on the Orion Crew Module (CM), it was determined that the CM deflects outward slightly due to the delta in pressure across the CM walls. Though a smaller impact, non-gravitational accelerations, known as G-loading, can also introduce this structural deformation. This phenomenon has been likened to a balloon expanding. When this slight deflection was modeled in simulation as a function of both atmospheric pressure and G-Loading, it was determined that the rate of deflection on reentry was significant enough to be measured as an angular rate by the Inertial Measurement Units (IMUs). The CM has three IMUs for redundancy; these IMUs are located at different locations across the vehicle. Due to the location of these IMUs, one IMU has the potential to rotate more during Ascent and Reentry compared to the other two when the structure deforms. This perceived rotation causes a false positive failure of the non-adjacent IMU by the IMU Fault Detection Isolation and Recovery (FDIR) algorithm, a subset of the overarching Navigation FDIR. Several solutions were investigated to solve for this false positive issue, while keeping Navigation FDIR sensitive to real faults. This paper looks to expound on the ballooning phenomenon, how this phenomenon negatively impacts the default IMUFDIR algorithm, the solutions investigated, the off nominal scenarios developed to validate the final solution, the tuning methodology of the updated IMUFDIR algorithm, and finally the results of the chosen solution and any future work.

[†]Orion Guidance Navigation and Control Engineer, Lockheed Martin - Space, Denver, CO

[‡]Orion Navigation MODE Team Engineer, EG/Aeroscience and Flight Mechanics Division, NASA -JSC Engineering Directorate, Houston, TX

BALLOONING PHENOMENON

Results of TVAC Testing

In TVAC Testing at the NASA Glenn Plum Brook facilities the Orion Capsule was slowly pressurized to reproduce the expected vacuum environment in Exo-LEO. This pressurization brought about slight structural deformation, visualized as ballooning or expanding of the vehicle. While smaller than the pressure-based deformation, FMEA analysis indicated that acceleration, i.e. G-loading, could also induce deformation on a similar order of magnitude. This deformation can be visualized in 1000x magnification in Figure 1. Reviewing the FMEA image, the vehicle has significant structural deformation along the middle horizontal strut of the vehicle. It is this strut which the IMUs are mounted to and is why the IMUs sense the localized structural deformation of this strut.

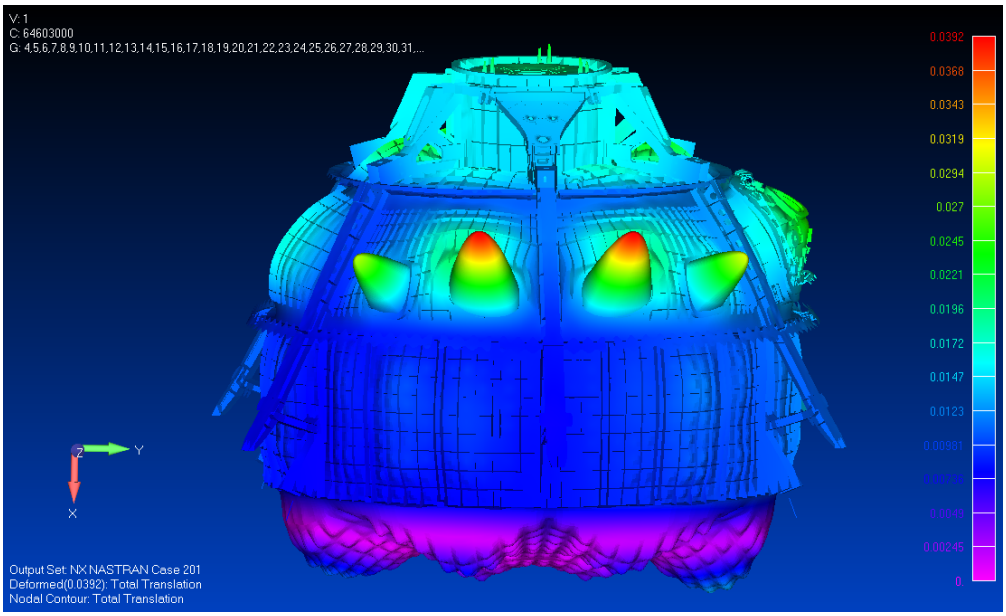

Figure 1. Orion Capsule Structural FMEA Analysis (Deformation Magnified 1000x)

The three IMUs are not co-located, with two IMUs oriented near one another on the middle strut and the third IMU located across the vehicle mounted on the same strut. The nonadjacent IMU is referred to as IMU-1. Given the orientation of the IMUs on the Orion Capsule, particularly IMU-1, the IMUs have the potential to move and rotate relative to each other due to structural flexing. This distance between the IMUs and their respective locations is depicted below in Figure 2.

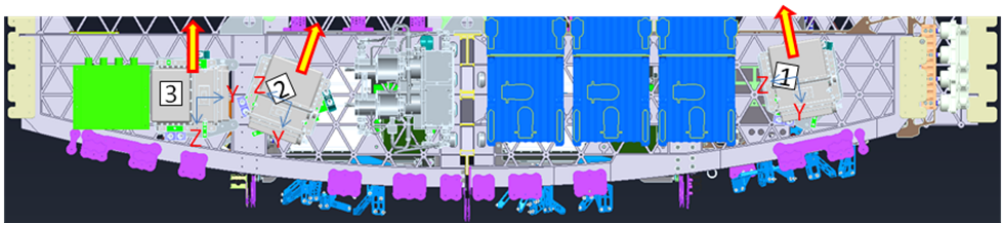

Figure 2. IMU Locations on Orion Capsule

It is this distance between IMUs which gives rise to an issue in the IMUFDIR algorithm, causing false

positive failures of an IMU in nominal flight. Though these movements are small, on the order of tenths of a degree, the IMU sensors and the IMUFDIR algorithm are sensitive enough to capture these movements, which will then be interpreted as 'errors' by the comparison algorithm within FDIR. This will be reviewed in more detail in the IMUFDIR Algorithm section.

Modeling in Simulation

Leveraging the structural analysis performed by the Orion Structures team, the location of the IMU Box bolt holes were captured both before and after ballooning due to pressure and G-Loading. Two assumptions were made in modeling the movement of the IMU Box as a function of pressure and G-Loading. First, given the results from the FMEA analysis, it can safely be assumed that translational motion has minimal impact on the Navigation FDIR system and Navigation sensors. Translation motion can therefore be ignored. This model exclusively focuses on the rotation of the IMU box induced by pressure and G-load. Second, the same rotation is assumed linear on the order of pressure changes and G-Loads anticipated in the environment the Orion Capsule will operate in. With these two assumptions the IMU relative misalignments were converted from point displacements, as delivered by the FMEA analysis, to transformation matrices to be represented as a change of frame from the 'Nominal' IMU Case Frame to the 'Deflected' IMU Case Frame. This transformation matrix is depicted in Eq. (3).

$$\gamma_{gload} = (a_{sensed}) * (\gamma_{Expected\,1G}) \tag{1}$$

$$\gamma_{press} = (\Delta P) * (\gamma_{Expected\,1Atm}) \tag{2}$$

$$T^{Deflected}_{Nominal} = Angle\_to\_Rotation\_Matrix(\gamma_{gload} + \gamma_{press})^{\dagger} \tag{3}$$

Eq. (3) can now be used to rotate from the 'Nominal' IMU Case Frame to the 'Deflected' IMU Case Frame.

Dispersions for Monte Carlo Analysis

To fully capture the uncertainty of this model update, variation was applied to the misalignment angles used to model the rotation as a result of Pressure and G-Loading. The FMEA performed by the Orion Structures team has a requirement of $\pm 10\%$ accuracy when modeling the observed deformations from testing. This motivated the dispersions used to capture the 1-G and 1atm misalignment angles. The parameters for the dispersion models are depicted below.

$$1G\,Misalignment\,Mean = \mu_g \tag{4}$$

$$1G\,Misalignment\,std = 3\sigma_g = 0.1 * \mu_g \tag{5}$$

$$1Atm\,Misalignment\,Mean = \mu_p \tag{6}$$

$$1Atm\,Misalignment\,std = 3\sigma_p = 0.1 * \mu_p \tag{7}$$

These parameters were used to model the perceived misalignments as two independent, normally distributed random variables. These dispersion models were used in the Monte Carlo analysis and results discussed in the Results section.

[†]Mathematical notations expounded upon in the Notations section

IMUFDIR ALGORITHM

The IMUFDIR algorithm is the main algorithm with the Navigation FDIR System for detecting and isolating IMU related faults. Because of this it is most impacted by the ballooning phenomenon. In the Orion Navigation Architecture there are three separately performing inertial sensors known as IMUs. These can be visualized in previous sections Figure 2. The IMUFDIR algorithm leverages the concept of parity to determine the inconsistency between the three IMUs during all phases of flight. The goal of the algorithm is to detect 'soft' failures, failures which are not identified by the Built-in-Tests (BIT) internal to the hardware's firmware. When a 'soft' failure is detected, the specific sensor must be isolated from the Navigation solution if that sensor continues to operate outside its design range. If that channel re-conforms to nominal behavior it has the potential to be recovered, reintroducing that channel to the Source Selection queue to potentially be selected for downstream use.

Preprocessing

All three sensors operate independently, passing ΔVs and $\Delta\theta$s into the IMUFDIR algorithm. These measurements must be processed before entering the Parity algorithm within IMUFDIR. For both ΔV and $\Delta\theta$ the measurements are synchronized to be on the same time step, as the three IMUs operate asynchronously. The measurements are then transformed out of their individual Case Frames to a common reference Frame defined as the IMUFDIR Frame. In the Orion System the IMUFDIR Frame sits at the mathematical center between all three IMUs, but it's location is arbitrary. Note, to move ΔVs to a different reference frame, a lever arm correction must be performed to account for the additional accelerations introduced via angular rates. These measurements are converted to real engineering units for parity by simply dividing the $\Delta Measurement$ by Δt. The last step of preprocessing is to filter the data leveraging a Low Pass Filter

Parity

Parity operates on the idea of capturing the inconsistency with the expected error of several measurements. If given two measurements with their associated errors, modeled as an additive error in the below example equations Eq. (10), parity then captures the expected difference between the pure error source, η. Note that for inertial navigation ϵ is a general term to model bias, scale factor, and noise related error terms, x1, x2, x3 represent the measured state of each of the three IMUs.

$$(x_1 + \epsilon_1) - (x_2 + \epsilon_2) = \eta_1 \tag{8}$$

$$(x_2 + \epsilon_2) - (x_3 + \epsilon_3) = \eta_2 \tag{9}$$

$$(x_1 + \epsilon_1) - (x_3 + \epsilon_3) = \eta_3 \tag{10}$$

$$Parity\,Vector = \begin{bmatrix} \eta_1 \\ \eta_2 \\ \eta_3 \end{bmatrix} \tag{11}$$

These three parity equations capture the parity equations for this system, where the state measured is the magnitude of the state, either acceleration or angular rate. This means three parity values - η_1, η_2, η_3 - make up the parity vector. The parity vector is used to estimate the discontinuity in measuring a 1-D value, magnitude of state. If a component of the parity vector spikes relative to the other two components of the parity vector, this means that the error, associated with that inertial sensor has increased relative to the error

observed in the other two inertial sensors. These parity values are not constant even in fault-free operation. Due to nominal misalignments in the mounting of the sensors, error as a function of state will enter the parity equation. Therefore, the parity vector is a dynamic vector, motivating the development of a dynamic Detection Threshold to be used for Detection and Isolation.

Detection Threshold

The Detection Threshold (DT) is the key to determining when the IMUFDIR algorithm will detect and isolate a fault. The Detection Threshold is a dynamic threshold as a function of both state and the anticipated 1-σ error of the inertial sensor. The gyroscope's modeled error are defined below in Table 1.

Table 1. Gyroscope Modeled Errors

Error Symbol	Description
σ_{GB+N}	1σ error budget value for gyro bias and gyro noise
σ_{GSF}	1σ error budget value for gyro scale factor
σ_{Gt}	1σ error budget value for gyro time skew

Besides 1-σ noise and bias error, since the parity vector can dynamically change as a function of state in nominal operation, the Detection Threshold must also change dynamically so that false positives are not signalled during high dynamic events, such as attitude maneuvers or Entry and Ascent. The full detection threshold as a function of both angular rate and angular acceleration is depicted below. Note that it is the angular rate, ω, and angular acceleration, $\dot{\omega}$, which make the Detection Threshold dynamic.

$$DT^2 = \sigma_{GB+N}^2 + \sigma_{GSF}^2 * (\omega_{avg} \cdot \omega_{avg}) + \sigma_{Gt}^2 * (\dot{\omega}_{avg} \cdot \hat{\omega}_{avg})^2 \tag{12}$$

This equation interacts with the parity vector Eq. (11). If an index of the parity vector spikes above the detection threshold a flag is thrown indicating that a fault was Detected. The state of the inertial sensor will change from 'Pass' to 'Suspect'. If that index of the parity vector is above the Detection Threshold for long enough, breaking the Persistence Limit, the health status of the inertial sensor will change from 'Suspect' to 'Failed'. Both the Gyroscope Parity Vector and its associated Detection Threshold along with Angular Rates can be seen in Figure 3.

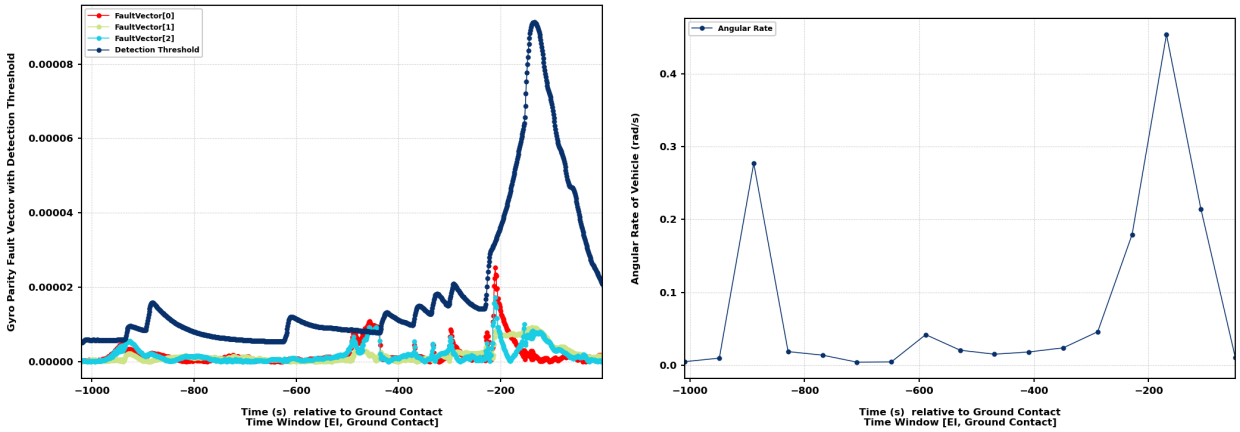

(a) Gyro Parity Vector and Detection Threshold **(b) Magnitude Angular Rate**

Figure 3. IMUFDIR Parity Vector and Detection Threshold as Functions of Angular Rate

Reviewing Figure 3 both the Parity Vector and Detection Threshold can be dissected further. At the beginning of the run the Detection Threshold is constant as the Angular Rates are Null, meaning that the Detection Threshold is only a function of the constant value σ_{GB+N}. Near the end of the run around 200 seconds before Ground Contact, the vehicle begins to spin and the angular rates increase. Because of this increase in state both the Parity Vector and the Detection Threshold spike, as anticipated. After the IMUFDIR algorithm is performed, the inertial measurements and their associated health status are then passed to the state estimation routine. Three independent navigation sources are then provided for selection. The Source Selection Algorithm is key for determining which source of the three to provide as the Navigation solution downstream. If the IMUFDIR Algorithm labels a channel as 'Suspect' that channel is moved to the end of the queue, and Source Selection will then select the next channel in its priority list. If the channel is then labeled as 'Failed' that channel will be removed entirely from the potential selectable channels for Source Selection. This means Detection is the key step for determining when a Channel is deselected by the Source Selection Algorithm. If a fault is detected that channel will immediately be deselected and have no negative impact on downstream users. If the fault persists, Isolation of the sensor and failing the channel will then follow, but this happens internally to the navigation software and is not as time critical compared to Fault Detection.

POTENTIAL SOLUTIONS

With Eq. (12) and Eq. (11) defined potential solutions to the ballooning phenomenon can be investigated. Due to structural deformation, one of the indices of Eq. (11) goes above the Detection Threshold, eventually failing the associated IMU. To combat this the IMU sensors could be re-positioned to the same location on the vehicle on a Navigation Bulkhead to minimize movement relative to one another. Given the late stage of the program when this phenomenon was discovered, redesigning the hardware orientation was not an option, making this solution impossible. Skewing the IMUs would help in implementation of some sort of Axis Based Parity algorithm, making the faults on individual sensors observable, but was not feasible in this system. However that option isn't practical for the same reason the IMUS could not be relocated to a common bulkhead. Given that the Detection Threshold is dynamic an additional term could be added for pressure, feeding back pressure as an additional dynamic term for the Detection Threshold to dynamically moved as a function of. This would let the Parity Vector spike but not break the Detection Threshold when pressurization occurs. Unfortunately pressure is not an available piece of sensor information for the IMUFDIR algorithm,

making this an unavailable solution. The two potential solutions that are worth investigating are tuning the σ_{GB+N} term within the Detection Threshold and tuning the Persistence Limit for the persistence counter when a fault is detected. Increasing σ_{GB+N} would allow for the detection threshold to bound the spike in the parity vector associated with ballooning. Increasing the persistence limit would stall isolation over the duration of deflection. Both of these solutions will be investigated in the following sections.

SCENARIOS

Evaluation of the Navigation FDIR capability includes assessment of GN&C key driving requirements and FDIR performance on scenarios which include mission critical events. Scenarios from the Artemis-2 re-entry phase were selected and expanded on for initial FDIR analysis and verification because GN&C criticality. During re-entry, GN&C is expected to perform automated guidance, targeting, and landing in order to safely return the vehicle. Two baseline re-entry scenarios were simulated using 6 DOF dynamics: nominal skip entry and ballistic entry. Each of these scenarios modeled deflection of the IMUs due both pressure to G-Loading. Additionally, the nominal skip entry scenario was modified to develop four new scenarios which contained a fault on either the gyro or accelerometer of the IMU. These four scenarios were specifically designed to test IMUFDIR, which were just a subset of all the scenarios developed to test Navigation FDIR. Testing IMUFDIR included six scenarios total, which were used to evaluate FDIR false positives, as well as FDIR performance when a fault is present. Only scenarios which are relevant to IMU deflection are discussed, which include the nominal skip entry, ballistic entry, and off-nominal scenarios which include fault injection on a gyro. The following sections contain details of each scenario and methodology used for fault selection.

Nominal Skip and Ballistic Entry Scenarios

Throughout re-entry the GN&C system is expected to perform autonomously, e.g. without manual piloting by crew. A crucial function of the autonomous capability is Navigation FDIR subsystem, since it protects the state estimate to guidance and control from corrupted sensor data. FDIR is expected to intervene only under the condition of a faulted or degraded sensor. Failing a nominally operating sensor is considered a false positive. False positives are to be avoided as they remove redundancy as well as degrade or eliminate the fault detection capability.

For re-entry, FDIR capability was assessed using the nominal skip and ballistic entry scenarios. The skip entry and ballistic scenarios were selected to assess IMUFDIR due to their differences in the vehicle structural deformation. Each entry altitude profile is visualized in Figure 4a, where each profile's altitude starts at Entry Interface (EI) and ends at ground contact. The skip entry altitude profile contains the signature dip in altitude where the vehicle flies through the atmosphere to aero-break and lower speed before re-entering the atmosphere. In comparison, the ballistic entry profile is also visualized in Figure 4a which directly enters the atmosphere.

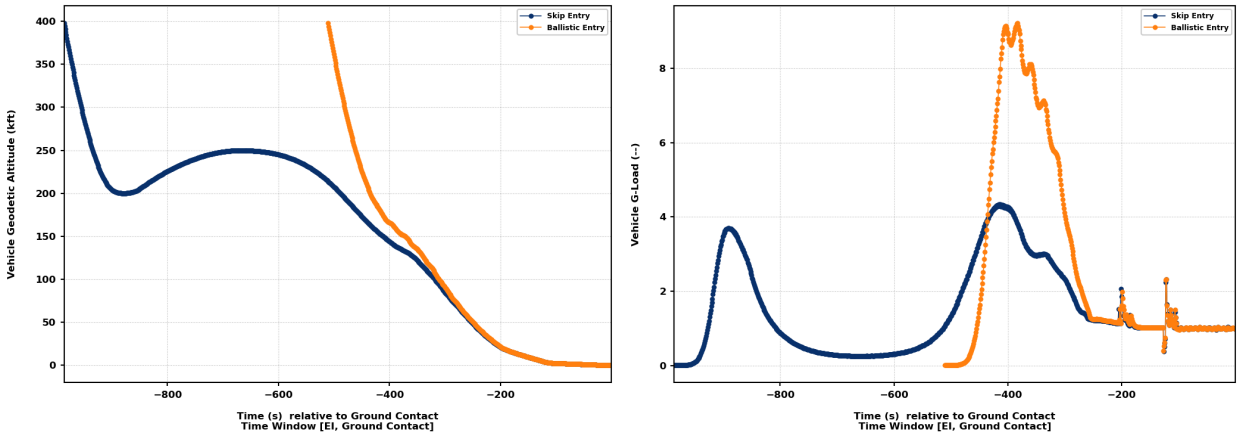

(a) Vehicle Geodetic Altitude **(b) Vehicle G-Load**

Figure 4. Vehicle States Influencing IMU Misalignment of the Skip and Ballistic Entry Profiles from Entry Interface to Ground Contact

Due to the direct entry, the vehicle has a faster speed than the skip out profile, and experiences larger non gravitational drag forces, thus higher G-Loads. The difference in G-Loads for each of the entry profiles is visualized in Figure 4b. Due to their similarity in altitude during the last 100 kft of descent, the profiles have comparable atmospheric pressure changes. Although the comparison of the two entry profiles was oversimplified, the noted variables are important to the structural deformation of the vehicle.

The structural deformation due to pressure differential and non-gravitational forces has the most potential to lead to false positives since both effects caused the IMUs to move relative to each other. The dynamic misalignment for each entry profile are co-plotted to illustrate the differences. The misalignment due to pressure and non gravitational forces are visualized in Figure 5.

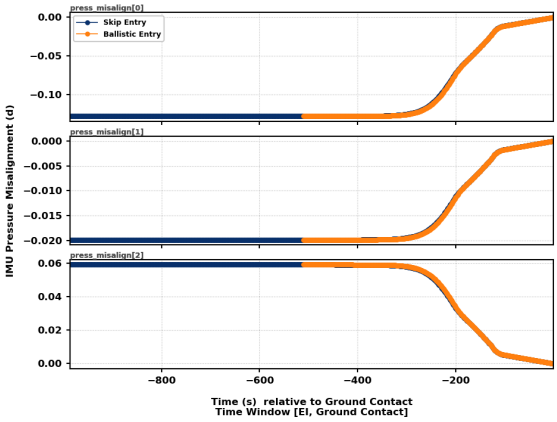

(a) IMU Misalignment By Axis Due to Pressure Differential

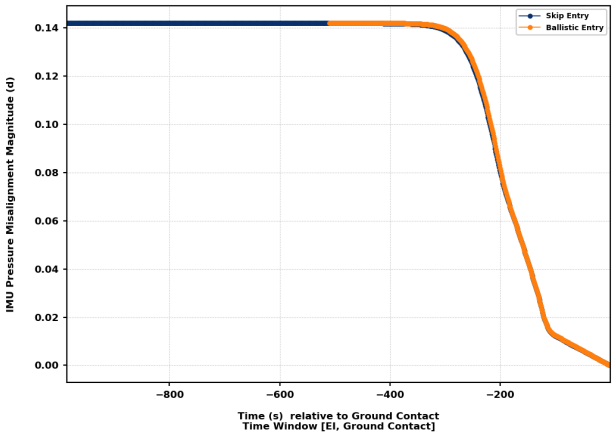

(b) IMU Misalignment Magnitude Due to Pressure Differential

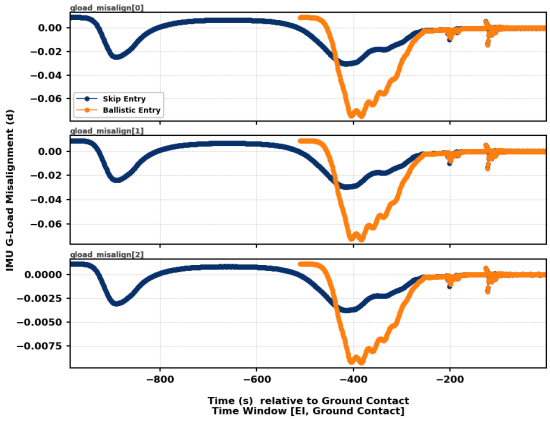

(c) IMU Misalignment By Axis Due to G-Load

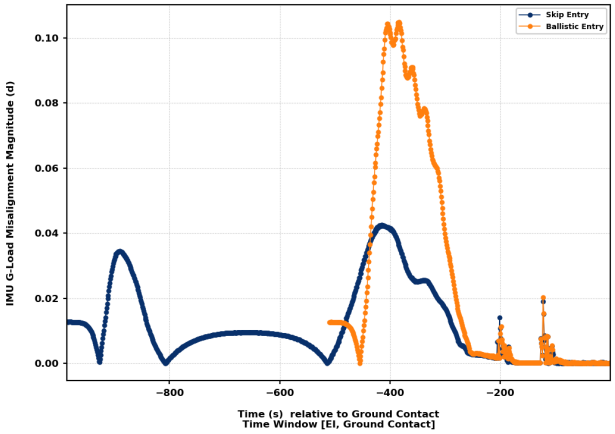

(d) IMU Misalignment Magnitude Due to G-Load

Figure 5. IMU Misalignments Due to and Pressure Differential G-Load of the Skip and Ballistic Entry Profiles from Entry Interface to Ground Contact

The main difference between the profiles is in non-gravitational misalignment, which is due to the high dynamics of the ballistic entry case. Visualized in Figure 6 is total misalignment between the two trajectories, where the main difference again is the contribution of non-gravitational forces in the ballistic entry scenario. Given the additional misalignment due to high non-gravitational forces, the ballistic entry scenario is the more stressing test of the FDIR algorithm. These two scenarios will test if the dynamic misalignments have been properly accounted for in IMUFDIR in order to avoid false positives.

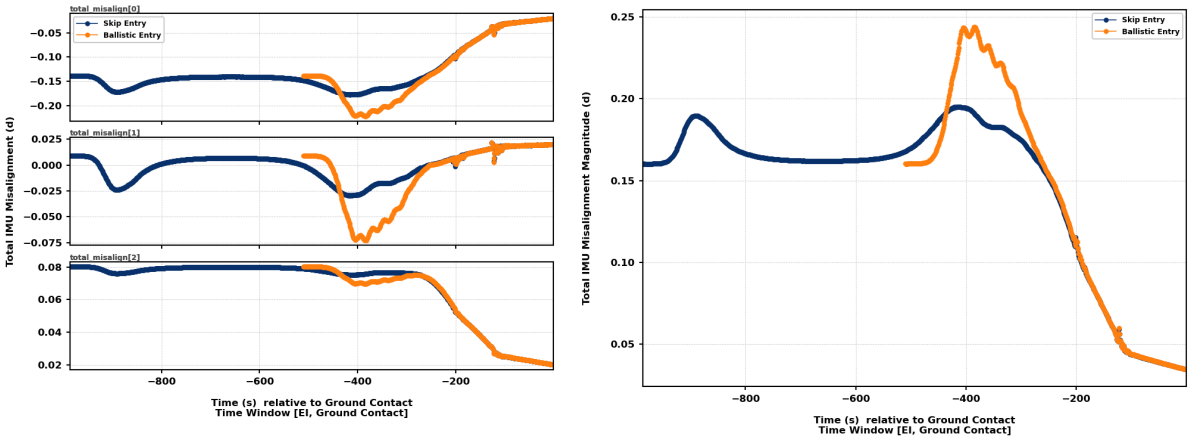

(a) Total IMU Misalignment By Axis **(b) Total IMU Misalignment Magnitude**

Figure 6. Total IMU Misalignments of the Skip and Ballistic Entry Profiles from Entry Interface to Ground Contact

Off-Nominal Scenarios and Fault Selection Methodology

The nominal skip entry scenario was used as a baseline for the development of two off-nominal scenarios used in the evaluation of IMUFDIR Gyro Parity. Each scenario contained a fault injection which changed the value of an error source of the simulated IMU model. The error sources considered for fault injection were gryo read out noise and single axis bias. Each fault was injected at various points in the base scenario to produce a catastrophic outcome. The fault value used for each of these error sources was selected based on a boundary value analysis approach.

All sensors are subject to error to an extent, however there is a non-zero probability which they will operate outside their hardware specifications. The purpose of FDIR is to protect the system from these instances, especially those where degraded or erroneous sensor data leads to an undesirable or catastrophic outcome. A fault which would cause a catastrophic event, such as loss of vehicle, mission, or life, would be necessary to verify FDIR capability. An exhaustive test of FDIR to all possible faults is impractical, so in order to select a fault, an investigation similar to a boundary value analysis was conducted. The investigation iterated over a range of fault values, to select one located on the fault domain boundary where the fault injection lead to a catastrophic outcome. The investigation was repeated for different types of fault, where the selected faults would then be used as an input to evaluate FDIR.

The setup for this investigation was simple given that a baseline entry scenario already existed. First, the scenario was modified with an event based trigger to inject the fault given specific vehicle state conditions. Second, the input to the scenario was modified in order to take fault values as arguments. Third, FDIR was inhibited and sensors were configured such that the system would be forced to use the faulted sensor. Finally, an automation script was set up to iterate over a range of fault values as input to the scenario. Each scenario was run using a different fault value, and the data generated could be assessed to determine which of these faults lead to a catastrophic outcome.

An example of such an assessment is given in Figure 7. In this scenario's fault investigation, a fault was injected prior to EI by changing the gryo read out noise to be greater than its specification value. This fault has the potential to result in a loss of vehicle due corrupted navigation data to guidance and control leading to non return trajectory, colloquially known as a skip out. The range of fault values considered is visualized in Figure 7a. For each of these fault values, vehicle geodetic altitude was inspected to assess skip

out, as shown in Figure 7b. The smallest value which resulted in a skip out is highlighted in orange in both data visualizations of Figure 7. This type of assessment was conducted to select faults for each off-nominal scenario.

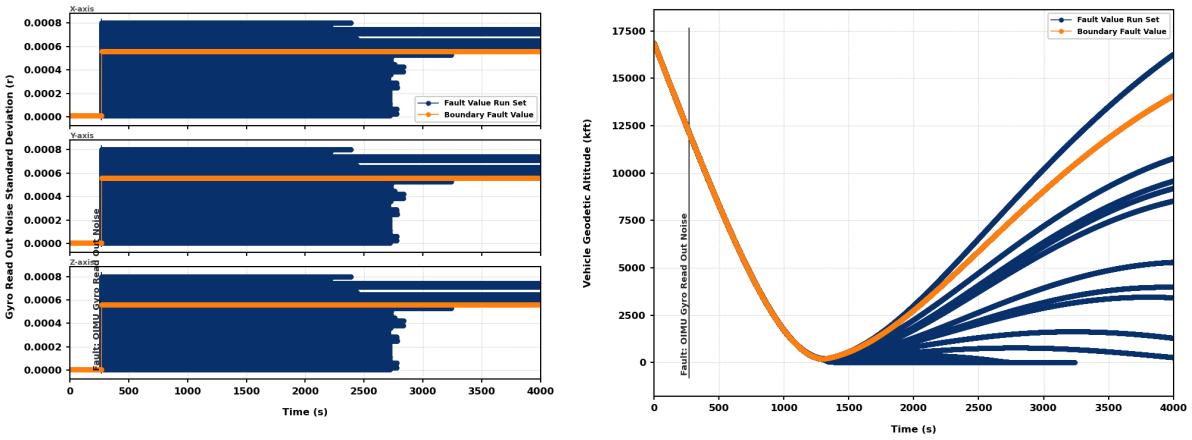

(a) Fault Values Investigated **(b) Altitude Displaying Skipouts**

Figure 7. Investigation of Gyro Read Out Noise Fault Values with Smallest Fault Value Leading to Skipout Highlighted

The evaluation of FDIR had a specific focus on IMUFDIR as it had recently undergone changes to accommodate the ballooning effect. The investigation considered pre-entry catastrophic events, those which could occur prior to EI, as well as faults which could occur during the descent and landing phase. Boundary values of faults were selected for gryo read out noise, which resulted in an entry skip out and gryo single axis bias, which resulted in failure of parachute deployment conditions. The faults selected from this investigation were directly used in scenarios that evaluated IMUFDIR Gyro Parity performance.

TUNING METHODOLOGY

The parameters in IMUFDIR gyro detection threshold given by Eq. (12) required tuning in order to prevent false positives due to structural deformation of the vehicle. The one parameter from the equation, the value for gyro bias and noise σ_{GB+N}, and two external model parameters, the *Persistence Limit* (PL), and the *Recovery Counter* (RC) were considered for tuning, each listed for quick reference in Table 2.

Table 2. Tuning Parameters Definitions

Tuning Parameter	Description
σ_{GB+N}	1σ error budget value for gyro bias and gyro noise
Persistence Limit (PL)	Number of cycles of detection required to isolate IMU
Recovery Counter (RC)	Number which persistence counter decrements when below detection threshold

Each parameter is first considered in isolation, as each will effect the performance of IMUFDIR. Adjusting σ_{GB+N} would shift the detection threshold and change both the initial detection speed and the sensitivity to small sensor faults. Increasing σ_{GB+N} would be one option to account for the ballooning phenomenon, since

it can be used to bound the parity vector's response to the structural deformation. An example of increasing σ_{GB+N} and how it shifts the detection threshold is visualized in Figure 8. In this illustration, two detection thresholds are given where the orange detection threshold represents an increase in σ_{GB+N} relative to the dark blue.

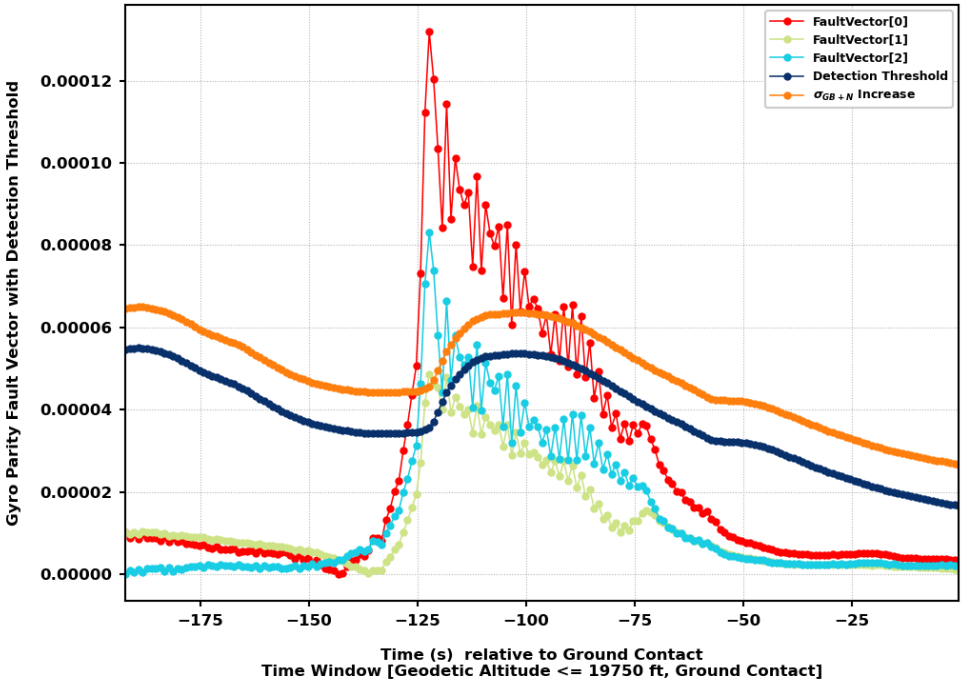

Figure 8. Gyro Parity Illustration of Increased σ_{GB+N} Tuning Parameter

Alternatively, adjusting the *Persistence Limit* would change the duration a fault component can remain above the detection threshold before IMUFDIR declares that component as failed. This adjustment would change the speed in which the algorithm would isolate. Increasing the *Persistence Limit* would also be an option to account for the ballooning phenomenon. Since the IMU deflection is a transient behavior, the duration in this which occurs can be estimated. Setting *Persistence Limit* to be greater than this duration would effectively bound the fault vector in time whenever structural deformation occurs. To illustrate *Persistence Limit*, a case where the gyro parity vector exceeds the detection threshold is given in Figure 9a with lines indicating different values of Persistence Counter. Each one of these lines indicate where IMUFDIR would perform Isolation if that had been the value of the *Persistence Limit*. Lastly, adjusting the *Recovery Counter* would change how much the Persistence Counter changes once a fault component drops back below the detection threshold. Changing this parameter also changes Isolation speed, but it also changes the time in which a component is not longer considered suspect. Figure 9b illustrates how the *Recovery Counter* effects the speed in which the Persistence Counter decreases once the fault vector component is below the detection threshold. The performance metrics in which these parameters change can be summarized as time to detection to time to isolation.

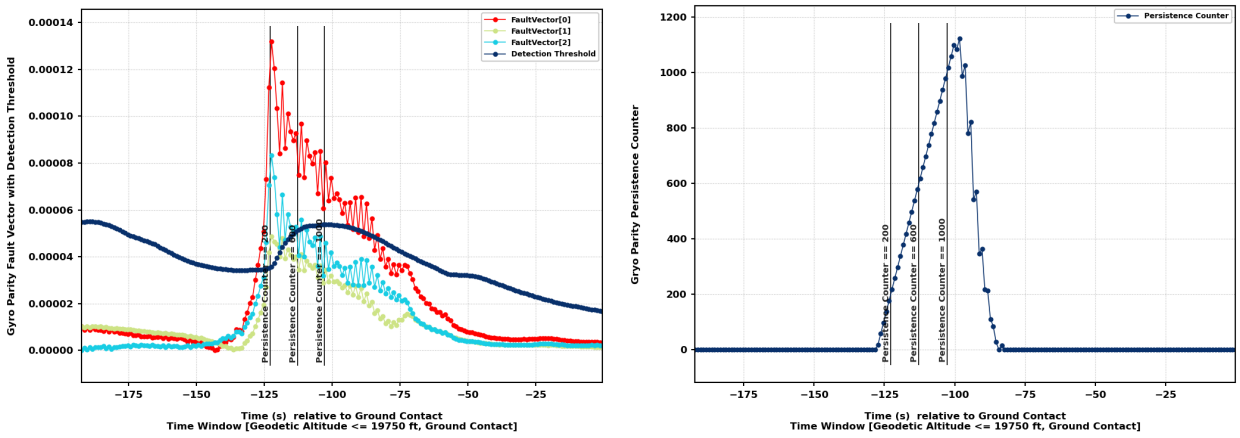

(a) Gyro Parity **(b) Persistence Counter**

Figure 9. Gyro Parity Illustration of Persistence Limit and Recovery Counter Tuning Parameters

The goal of IMUFDIR tuning is to adjust σ_{GB+N}, *Persistence Limit*, and *Recovery Counter* parameters in order to reduce the number of false positive failures due to structural deformation while still maintaining Detection and Isolation against potential catastrophic faults. The nominal and skip entry scenarios mentioned in Section were used to assess number of false positives while the off-nominal scenarios mentioned in Figure were used to assess Detection and Isolation performance. The scenarios were run in Monte Carlo simulation without any tuning updates to establish baseline performance. From this baseline data set, the worst performing runs were selected for tuning. A parameter search method was used to conduct tuning, where a each selected run was rerun over a range of tuning parameter values. The data set was mined to find the set of tuning parameters which eliminated false positives while successfully detecting and isolating catastrophic faults. With the parameter set that was selected, each scenario was rerun using Monte Carlo simulation, and the process of parameter search was applied again on worst performing runs. This process was repeated until the false positive probability was under 0.27%, and IMUFDIR was able to Detect and Isolate the faults with a probability of success of 99.73%, each with a confidence interval of 90 %.

Another aspect to consider during tuning is the design of the the Navigation FDIR system as a whole, that which extends past the domain of IMUFDIR. Whenever any individual sensor FDIR initially Detects an issue, that sensor is reported as suspect to Source Selection. Source Selection will de-prioritize any channel with suspect sensor measurements, and will maintain state estimates output from channels with healthy sensors. Due to this design, reducing the time of initial detection is preferred, since it protects guidance and control from potentially using a faulty navigation state. In the context of the tuning exercise, this means selecting a parameter set which not only meets false positive probability, Detection and Isolation criteria, but also prioritizes time to Detection over time to Isolation.

TUNING RESULTS

With the IMU model updates, scenarios, and tuning methodology defined and in place, simulations were run using Monte Carlo methods in order to assess performance. The nominal skip entry and ballistic entry scenarios were run to establish a baseline with respect to false positives. The percent of runs for each scenario which IMUFDIR detected the deflection of IMUs due to structural deformation, and the percentage in which a false positive occurs are listed in Table 3. The ballistic entry scenario has a higher rate of false positives, this is primarily due to higher non-gravitational forces relative to the nominal skip entry.

Table 3. Pre-Tuning Percent False Positives for Monte Carlo Sample of 3000

Scenario	Percent Detection	Percent False Positive
Nominal Skip Entry	48.90	4.10
Ballistic Entry	38.07	26.37

These same scenarios were run again with IMUFDIR isolation capability inhibited, which enabled assessment of the duration in which IMU deflection affected detection. As described in the IMUFDIR Algorithm, detection occurs when a component of the fault vector is greater than the detection threshold. When isolation occurs, this fault component is removed from the parity algorithm. By inhibiting isolation, it allows for the behavior of the fault vector to be assessed through all occurrences of structural deformation. The fault vector for both nominal skip entry and ballistic entry scenarios is visualized in Figure 10. By inspection, the ballistic entry scenario has a much larger duration in which the parity vector exceeds the detection threshold. If the isolation was again enabled, the *Persistence Limit* would need to be greater than this duration in order to prevent a false positive from occurring.

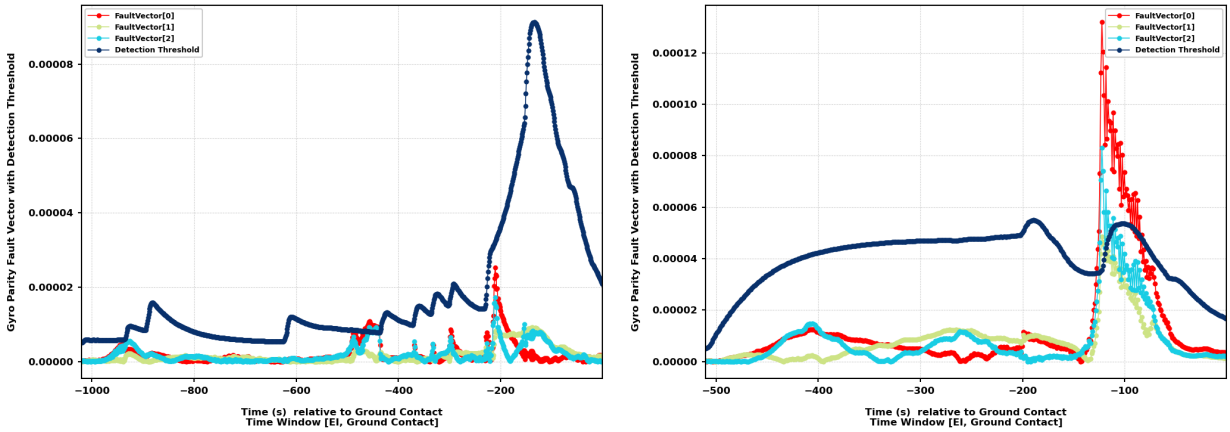

(a) Nominal Skip Entry **(b) Ballistic Entry**

Figure 10. Gyro Parity of Nominal Skip and Ballistic Entry with IMUFDIR Inhibited from Entry Interface to Ground Contact

When isolation is inhibited, the Persistence Counter continues to increment past the *Persistence Limit* whenever an IMU fault vector component is above the detection threshold. For each run in the Monte Carlo which had a detection event, the maximum of the Persistence Counter was obtained to inform the tuning of the *Persistence Limit*. Visualized in Table 4 is the maximum of the Persistence Counter for each data set as a box plot, as well as mean, standard deviation, and quartiles. The count of each data set is different given that the percentile of detections, as stated is in Table 3 is different. The box plot illustrates that the largest outlier of the skip entry scenario is less than the majority of the outliers in the ballistic entry scenario. Therefore, adjusting the *Persistence Limit* to account for the number of false positives in the ballistic entry scenario will also bound the nominal skip entry scenario.

Table 4. Entry Scenario Box Plot, Descriptive Statistics and Percentiles for Persistence Counter

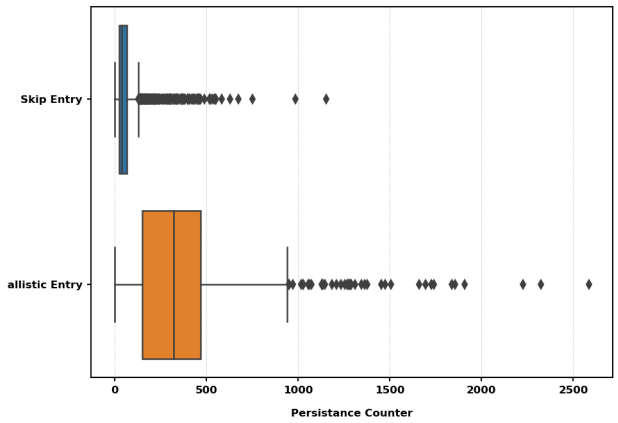

	Skip Entry	Ballistic Entry
Count	1467	1142
Mean	71.69	355.20
STD	101.47	288.73
Min	1	1
25%	23	150
50%	37	322
75%	66	467
Max	1154	2586

The fault vector and Persistence Counter analysis established a baseline for IMUFDIR parameter tuning of the *Persistence Limit*. Note that this baseline used a value for σ_{GB+N} which was representative of the hardware specification. If this value were to change, which it will for the tuning analysis, the Persistence Counter analysis would need to be repeated to find the bounding *Persistence Limit*. For tuning of σ_{GB+N}, a range of values were run with the worst performing cases in the off-nominal scenarios. The range of values for tuning σ_{GB+N} were split into 50 even steps, starting with the hardware specification and stopping at 16 times the hardware specification. For the following data visualizations, this is represented as **SBN#**, where **#** represents the index within the range with **SBN1** being the value of σ_{GB+N} and **SBN50** being $16 \times \sigma_{GB+N}$.

The worst performing cases in the off-nominal scenarios were determined by running a Monte Carlo of 3000 samples for each scenario with the top of the range **SBN50**. From the data set, a number of cases were identified where IMUFDIR failed to detect and isolate the fault, as well as instances of catastrophic outcomes due to slow fault detection. These cases were only identified in the off-nominal scenario which injected a gyro read out noise fault. From the failed cases, those which had the largest time to detect a fault were selected and rerun over the range of **SBN** values. Over the range of **SBN** values, only **SBN1** through **SBN27** were successful in detecting the faults withing a time frame which protected against a catastrophic outcome. The cases which had the largest Persistence Counters for the ballistic scenario were rerun over the new range of **SBN#**, from **SBN1** to **SBN27** in order to establish a bounding *Persistence Limit* for each index.

Over the range of **SBN1** to **SBN27**, the **SBN4** data stood out as it indicated a noticeable increase in time to detection performance in the subset of off-nominal reruns. Once a new *Persistence Limit* was established for each index, only **SBN1**, **SBN27**, and **SBN4** were used in a rerun of a full Monte Carlo of the off-nominal scenario of the gyro noise fault. Upon inspection of data, **SBN1** failed to isolate the faults on two runs. These two runs were rerun over a range of *Recovery Counters* to assess improvement in isolation performance. A Recover Counter value from this assessment was selected to generate another Monte Carlo data set with **SBN1**. Time to detection and time to isolation were computed for each data set generated in the gyro noise fault off-nominal scenario. The box plot of these times for each scenario is visualized in Figure 11 and the statistics in which these visualizations contain are tabulated in Table 5 and Table 6. In each of these data visualizations, the tuning parameters are abbreviated where **SBN#** represents the index used in the range of σ_{GB+N} values, **RC#** represent the *Recovery Counter* value used, and **PL#** represents the *Persistence Limit* value used.

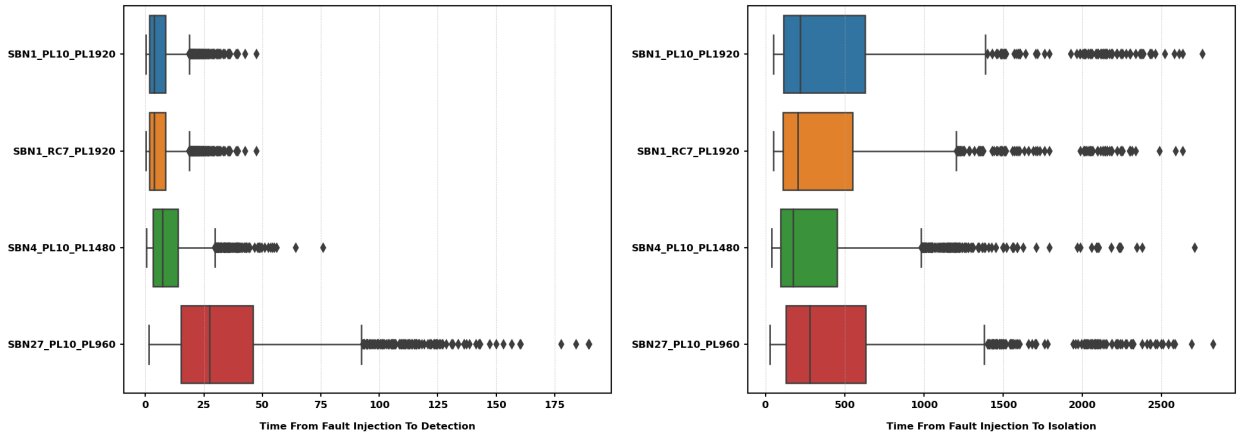

(a) Time to Detection **(b) Time to Isolation**

Figure 11. Box Plots of Detection and Isolation Times of Select Tuning Options

From inspection of Figure 11, there is a positive correlation between **SBN** and time to detection. This is due to σ_{GB+N} being additive in Eq. (12). Increasing the value of σ_{GB+N} effectively increases the detection threshold, making the algorithm less sensitive to faults. However, the lower **SBN**, the larger the *Persistence Limit* needs to be, thus increasing the time it takes to isolate a fault. Increasing **SBN** past the hardware specification desensitizes the fault detection algorithm. For instance, from inspection of Figure 11a red box plot, **SBN27** time to detection whisker extends out to past 90 seconds, and from Table 5, has a maximum detection time of approximately 190 seconds. **SBN27** worked for these scenarios, but 90-190 second range may not work for scenarios not yet engineered. The Navigation FDIR system as a whole prefers a time to detection over time to isolation, as initial detection prompts Source Selection to switch IMUs. Therefore, although **SBN4** performs better in duration it takes to isolate the faulted IMU, **SBN1** with **RC7** was ultimately selected due its better performance in time needed to detect the fault and its improved isolation performance relative to **SBN1** with **RC10**.

Table 5. Tuning Cases Descriptive Statistics and Percentiles for Time to Detection

	SBN1_RC10_PL1920	**SBN1_RC7_PL1920**	**SBN4_RC10_PL1480**	**SBN27_RC10_PL960**
Count	3000	3000	3000	3000
Mean	6.13	6.13	10.10	34.34
STD	6.33	6.33	9.08	26.32
Min	0.25	0.25	0.35	1.50
25%	1.68	1.68	3.28	15.07
50%	3.68	3.68	7.33	27.41
75%	8.46	8.46	13.86	46.03
Max	47.53	47.53	76.08	189.78

Table 6. Tuning Cases Descriptive Statistics and Percentiles for Time to Isolation

	SBN1_RC10_PL1920	SBN1_RC7_PL1920	SBN4_RC10_PL1480	SBN27_RC10_PL960
Count	2998	3000	3000	2997
Mean	421.78	378.13	319.94	440.81
STD	437.01	386.82	331.93	430.38
Min	48.88	48.88	38.23	29.63
25%	115.00	110.19	96.00	127.83
50%	218.31	205.23	176.03	279.33
75%	628.82	548.85	451.47	632.33
Max	2756.13	2634.08	2710.00	2824.55

The parameter set of **SBN1 RC10 PL1920** provided adequate fault detection and isolation for off-nominal scenarios with a probability of success of 99.73% each with a confidence interval of 90%. Furthermore, it reduced the false positive probability to be under 0.27%. Final results for detection and isolation for this parameter set are given in Table 5 and Table 6 respectively, where Count indicates the number of runs in the Monte Carlo which were successful in fault detection or isolation. The results of false positive percentages are provided for both the nominal skip entry and ballistic entry scenarios in Table 7. Although the tuning analysis brought the design back to using the hardware specification σ_{GB+N}, it provided insight into the design space and led to an informed design decision by providing rationale for selection of *Persistence Limit* and *Recovery Counter*.

Table 7. Post-Tuning Percent False Positives for Monte Carlo Sample of 3000

Scenario	Percent Detection	Percent False Positive
Nominal Skip Entry	48.90	0.00
Ballistic Entry	38.07	0.01

CONCLUSION

Structural Deformation was observed in TVAC Testing of the Orion Capsule. This structural deformation, mainly as a function of pressure changes and G-Loading, has the potential to cause false positive failures of the IMUs by the IMUFDIR Algorithm, due to the locations of the IMUs across the Orion vehicle. The solution presented in this paper is to lean on the Persistence Limit of the IMUFDIR algorithm, keeping an IMU in the 'Suspect' state longer before finally declaring that sensor 'Failed'. The benefit in this approach is the algorithm can still detect small faults in the inertial sensors while not failing a channel during 'Nominal' error induced by structural deformation. This solution was successful in driving false positive failures to zero while still meeting all Detection and Isolation requirements of the Navigation FDIR System when tested with real IMU related faults.

All of the testing was performed specifically on the Entry portion of flight. A similar effort needs to be allocated to the Ascent portion of flight, specifically Ascent Abort scenarios where the G-Loads can be significant and atmospheric pressure changes are still at play.

ACKNOWLEDGMENTS

Like any piece of work, technical or otherwise, it takes a team of dedicated individuals to accomplish challenging endeavours. This work is no exception. The authors of this manuscript would like to thank the dedicated engineers and navigators on the Orion Program. Specifically, thank you to Jesyca Fuenmayor-Bello, Robert Gillis, and Amritpreet Kang as their preliminary work helped to motivate this paper's findings.

NOTATION

γ_{gload}	misalignment due to sensed accelerations
$\gamma_{Expected1G}$	anticipated misalignment due 1-G of sensed accelerations
γ_{press}	misalignment due to pressure differential
$\gamma_{Expected1Atm}$	anticipated misalignment at 1 Atm of pressure
$T_{nominal}^{Deflected}$	Transformation Matrix capturing the rotation of the IMU sensor box due to Structural Deformation
μ_g	mean of 1-G misalignment
σ_g	standard deviation of 1-G misalignment
μ_p	mean of 1 Atm misalignment
σ_p	standard deviation of 1 Atm misalignment
x_n	true state index n (where n can be any integer 1-3)
ϵ_n	measurement error index n (where n can be any integer 1-3)
ν_n	parity index n (where n can be any integer 1-3)
σ_{GB+N}	1 standard deviation error budget value for gyro bias and gyro noise
σ_{GSF}	1 standard deviation error budget value for gyro scale factor
σ_{Gt}	1 standard deviation error budget value for gyro time skew
ω_{avg}	average angular velocity of the vehicle, averaged across three IMU measurements
$\dot{\omega}_{avg}$	average angular acceleration of the vehicle, averaged across three IMU measurements
$\hat{\omega}_{avg}$	unit vector of ω_{avg}

REFERENCES

[1] Collins, G., and Johnson, T. V., "Encyclopedia of the Solar System," *Ganymede and Callisto*, Elsevier Inc., Massachusetts, 2014, pp. 813–829.